"It doesn't matter how beautiful your theory is, it doesn't matter how smart you are. If it doesn't agree with the experiment, it's wrong."

– Richard P. Feynman

CHAPTER 4

EXCLUSIVE VECTOR MESON PRODUCTION THROUGH BK EVOLUTION

Exclusive diffractive processes, such as exclusive vector meson production, serve as excellent probes of hadron structure within the perturbative regime of quantum chromodynamics (QCD). The exclusive process involving light and heavy vector mesons, $ep \to eV(V = J/\Psi, \rho, \phi)$, has been investigated at the HERA accelerator facility. In this chapter, we focus on the theoretical prediction of exclusive J/Ψ and ρ^0 vector meson production. Employing the color dipole description of deep inelastic scattering (DIS), we calculate both the differential cross-section and total cross-section for the electro-production of J/Ψ and ρ^0 vector mesons, using an analytical solution to the Balitsky-Kovchegov (BK) equation. Furthermore, we present the ratio of the longitudinal to the transverse cross-section for the production of J/Ψ and ρ^0 as a function of Q^2. Two well-known vector meson wave function models, Boosted Gaussian (BG) and Gaus-Light Cone (GLC), have been integrated into our analysis, showing slight sensitivity to the chosen vector meson wave functions. Our theoretical predictions agree well with the available experimental data for vector meson production. The analytical solution of the BK equation proves reliable for the

theoretical prediction for the production of exclusive vector mesons within a specific range of Q^2. This chapter is based on the arXiv preprint: ***[arXiv:2405.07234]*** *(In communication).*

4.1 Introduction

Quantum chromodynamics (QCD), recognized as the quantum field theory of the strong force, elucidates interactions between hadrons. At short distances, corresponding to low values of the strong coupling constant α_s, perturbative QCD (pQCD) effectively predicts the dynamics of strong interactions among quarks and gluons. Numerous deep inelastic scattering (DIS) experiments conducted on hadrons by leptons at the experimental location have provided significant insights into the distribution of partons within hadrons (see to Ref. [1] for a review). The intricate structure of protons at the parton level has been examined in electron-proton collisions at the Hadron Electron Ring Accelerator (HERA). HERA has demonstrated a fast escalation in gluon density at small-x [2, 3]. This increase cannot persist indefinitely without contravening the Froissart bound and unitarity. Consequently, nonlinear dynamics become relevant to nuclear structure as x approaches minimal values. At small-x, gluon concentrations increase significantly, so that the diminutive nature of α_s is offset by the elevated gluon density. pQCD can be employed to characterize nonlinear dynamics in high-density QCD.

Color glass condensate (CGC) is a resilient QCD theory formulated to address nonlinear dynamics in high-density QCD. The CGC theory explains how gluons behave in a nucleus traveling at speeds close to that of light. It accounts for gluon saturation, forecasts the initial conditions of heavy-ion collisions, and streamlines quantum chromodynamics (QCD) calculations through effective field theory methods. The term "color" pertains to the attribute of the strong force, which is dictated by

QCD. The "glass" portion of CGC is based on an analogy with disordered materials, such as spin glasses. The gluons within a rapidly moving nucleus appear immobilized over very short timeframes due to time dilation, much like atoms in a glass remain disordered yet stationary over extended durations. The term "condensate" implies that the gluons are densely packed. CGC operates in the proton saturation region at small-x, illustrating the nonlinear saturation behavior of gluons within protons. Despite its success in describing nonlinear physics at small-x, we are still far from having strong evidence of the nonlinear saturation effect at present collider facilities. Some future facilities are being developed, including the Eletron-Ion Collider (EIC) in the United States [8], the Large Hadron electron Collider (LHeC) at CERN [9, 10], and the Eletron-Ion Collider in China [11]. In these future experimental facilities, the nonlinar effects will be easily accessible as the proton will be replaced by a heavy nucleus, so that parton densities enhance nearly $A^{1/3}$ in heavy nuclei. With these advancements, future facilities are expected to address the gluon saturation phenomenon and explore other QCD aspects associated with it.

In high-energy scenarios, diffractive processes serve as valuable tools for exploring the nonlinear dynamics of QCD in DIS experiments. A diffractive process in the context of high-energy QCD denotes a scattering process where a particle interacts with a target and leaves mostly intact (or only slightly modified) while generating a system with a significant rapidity gap, an area in phase space devoid of particles. These processes shed light on gluon saturation, the Color Glass Condensate (CGC), and pomeron exchange, enhancing our understanding of hadron structure within QCD. Diffractive processes, like the exclusive production of vector mesons, are especially effective for investigating the internal composition of hadrons, such as protons, in the saturation regime at low values of x [12–14]. In these operations, there is no net transfer of color charge, requiring the exchange of two gluons with the target hadron at the amplitude level. As a result, the cross-section becomes

responsive to the gluon density, and nonlinear dynamics are anticipated to emerge through exclusive mechanisms. Moreover, exclusive processes such as vector meson production distinctly allow for the computation of the entire momentum transfer to the target, hence aiding in the examination of generalized parton distribution functions (GPDFs). [15, 16] and the spatial configuration of target nuclei [17, 18].

Recent years have witnessed both theoretical and experimental endeavors aimed at the production of vector mesons. The ZEUS and H1 partnerships at the HERA accelerator facility have conducted investigations on vector mesons (J/Ψ, ρ, ϕ). The LHCb collaboration at CERN's LHC has supplied high-precision data on exclusive J/Ψ production in pp collisions at energies of $\sqrt{7}$ TeV and $\sqrt{13}$ TeV [25, 26], as referenced in [19–24]. The Golec-Biernat and Wusthoff (GBW) model [27], a seminal contribution from two decades prior, concentrates on the investigation of gluon saturation effects through diffractive deep inelastic scattering (DIS) processes at HERA, utilizing Mueller's dipole framework [28]. Comprehensive studies have been undertaken to examine the gluon saturation phenomenon by diffractive deep inelastic scattering mechanisms. Like the GBW model, the Color Glass Condensate (CGC) model addresses gluon saturation effects by characterizing the dipole scattering mechanism. Two impact parameter models, the IP-Sat [30] and b-CGC [31] models, have been utilized to evaluate if exclusive vector meson production acts as a sensitive indicator of gluon saturation at small-x. The above mentioned models are utilized to investigate vector meson generation in proton-proton and nucleus-nucleus collisions at the LHC experiment [32]. The results indicated that gluon saturation models offer a qualitative interpretation of the experimental findings.

To analyze any diffractive DIS process such as vector meson production, the color dipole model of DIS [28, 33–35] serves as a powerful tool. The color dipole description of e-p DIS with two gluon exchanges is depicted in Figure 4.1. In the color dipole model, electron-proton deep inelastic scattering can be articulated as

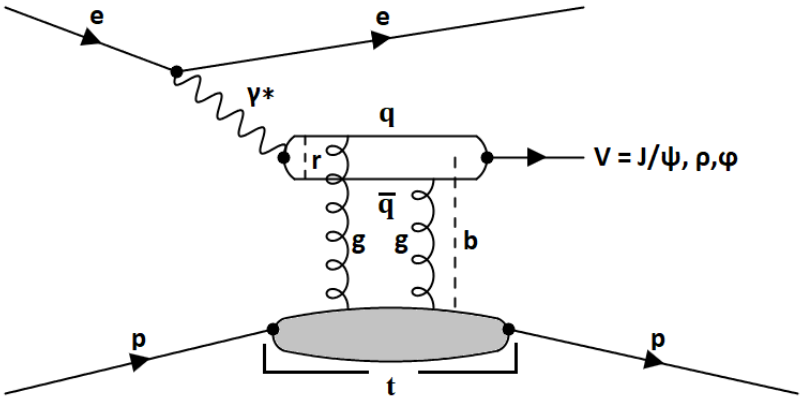

Figure 4.1: The exclusive vector meson production within the pQCD approach in the color dipole description of e-p DIS via two gluon exchange.

follows: The electron first interacts with the target proton through the exchange of a virtual photon. The virtual photon subsequently bifurcates into a quark-antiquark dipole prior to engaging with the proton and undergoing scattering through gluon exchange. Ultimately, the dipole recombines, resulting in the generation of final-state particles such as vector mesons or photons. The GBW model, CGC model, and CGC-based models accurately characterize the dipole scattering mechanism within this framework. The saturation effect in the IP-Sat and b-CGC models pertains to the DGLAP (Dokshitzer-Gribov-Lipatov-Altarelli-Parisi) equation and the BFKL (Balitsky-Kuraev-Fadin-Lipatov) equation, respectively. The progression of dipole-target scattering amplitude is mostly dictated by the BK (Balitsky-Kovchegov) equation, which characterizes gluon saturation through a nonlinear term. The BK equation serves as a mean-field approximation of the intricate JIMWLK (Jalilian-Marian-Iancu-McLerran-Weigert-Leonidov-Kovner) equation. Notwithstanding various numerical investigations [36–40], an exact analytical solution to this equation continues to be unattainable owing to its intricate character.

We recently introduced an approximate analytical solution to the BK equation, which is beneficial for phenomenological studies in the realm of nonlinear dynamics in high-density QCD [41]. This method has been effectively utilized to evaluate

the proton structure function F_2^p inside designated kinematic domains of x and Q^2 at HERA [42]. In Ref. [40, 43], the exclusive production of vector mesons has been examined using a numerical resolution of the BK equation. This study use the analytical solution of the BK equation to examine the exclusive vector meson production process and its dependency on several scales involved. In the color dipole framework of deep inelastic scattering (DIS), we evaluate the theoretical predictions for exclusive vector meson ($J/\Psi, \rho^0$) production, encompassing: (i) the differential cross-section with respect to the four-momentum transfer squared at the proton vertex t, and (ii) the total cross-section as functions of the center-of-mass energy of the photon-photon system W, and the virtuality of the exchanged photon Q^2. The new part of this study is that one component for measuring exclusive vector meson production within the color dipole framework is derived from the analytical solution of the BK equation.

The chapter is structured as follows: In Section 4.2, we examine and evaluate the color dipole framework of exclusive vector meson production in the e-p deep inelastic scattering process. In Section 4.3, we provide the theoretical calculation of the differential and total cross-sections for the production of J/Ψ and ρ^0 vector mesons in the process $ep \to epV$ ($V = J/\Psi, \rho^0$), taking into account the various scales involved. Additionally, this section presents the ratio of the longitudinal to the transverse cross-section the production of J/Ψ and ρ^0 as a function of Q^2. We compare our theoretical findings with current experimental evidence on vector meson generation. Section 4.4 offers an overview of the chapter.

4.2 Exclusive Vector Meson Production within Color Dipole Description of DIS

In this section, we briefly review and discuss the dipole description of e-p DIS for the electro-production of exclusive vector mesons. We first provide the dipole scattering amplitude for exclusive vector mesons production within the CGC framework. We then discuss wavefunctions for vector mesons, which are a key portion of the dipole description of DIS for vector meson production.

4.2.1 Dipole Scattering Amplitude for Vector Mesons

In the color dipole framework of deep inelastic scattering (DIS), a basic electron-proton DIS process [$ep \to epV$ ($V = J/\Psi, \rho, \phi$)] is seen as the interaction between the color dipole (quark-antiquark pair) and the target proton. The dipole scattering amplitude for exclusive vector mesons comprises three components: the photon wave function, the dipole-proton scattering amplitude, and the vector meson wave function. A schematic illustration illustrating exclusive vector meson creation within the pQCD framework, utilizing the color dipole model of electron-proton deep inelastic scattering by two gluon exchange, is presented in Figure 4.1. The transverse dimension of the quark-antiquark pair is denoted as $\mathbf{r}$, whereas $\mathbf{b}$ represents the impact parameter for the dipole-proton interaction. The quark possesses a fraction of momentum (z) of the photon's light-cone momentum, while the antiquark possesses ($1 - z$). In the perturbative regime, characterized by smaller dipole sizes (r), the dipole-proton cross section is associated with the exchange of a gluon ladder. In the proton's rest frame, the imaginary component of the scattering amplitude for exclusive vector meson generation within the dipole framework can be expressed

as [44]

$$\mathcal{A}_{T,L}^{\gamma^* p\to Vp}(x,Q^2,t) = i\int d^2\mathbf{r}\int_0^1 \frac{dz}{4\pi}\int d^2\mathbf{b}(\Psi_V^*\Psi)_{T,L}e^{-i\mathbf{b}.\boldsymbol{\Delta}}\times 2[1-S(x,r,b)]. \tag{4.1}$$

Here x represents the Bjorken variable, while Q^2 denotes the virtuality of the photon. The symbol $\boldsymbol{\Delta}$ represents the transverse momentum lost at the proton vertex by the outgoing proton, which is correlated with the squared momentum transfer as $t = -\boldsymbol{\Delta}^2$. Ψ denotes the wave function for the incoming photon in the process, a well-established concept in quantum electrodynamics (QED). Ψ_V^* is the wave function for the final state vector meson. $(\Psi_V^*\Psi)_{T,L}$ represents the overlap of the wave functions between the photon and the vector meson, where T signifies transversely polarized particles and L signifies longitudinally polarized particles. This expression quantifies the probability amplitude for the virtual photon to produce an exclusive vector meson or a real photon in the final state in e-p DIS within the framework of the color dipole description.

The scattering amplitude shown in Eq. (4.1) contains only the forward component of the amplitude. To have the non-forward scattering amplitude, we multiply the usual forward wave functions by an exponential factor, $\exp[\pm i(1-z)\mathbf{r}.\boldsymbol{\Delta}/2]$, following the work done by Bartels et. al. [45]. Following this change, together with the assumption that the S-matrix is purely real, we may write the scattering amplitude Eq. (4.1) as

$$\begin{aligned}
&\mathcal{A}_{T,L}^{\gamma^* p\to Vp}(x,Q^2,t)\\
&= i\int d^2\mathbf{r}\int_0^1 \frac{dz}{4\pi}\int d^2\mathbf{b}\,(\Psi_V^*\Psi)_{T,L}\,e^{-i[\mathbf{b}-(1-z)\mathbf{r}].\boldsymbol{\Delta}}\cdot\frac{d\sigma_{q\bar{q}}}{d^2\mathbf{b}}\\
&= i\int_0^\infty dr(2\pi r)\int_0^1\frac{dz}{4\pi}\int_0^\infty db(2\pi b)(\Psi_V^*\Psi)_{T,L}J_0(b\Delta)J_0([(1-z)r\Delta])\frac{d\sigma_{q\bar{q}}}{d^2\mathbf{b}},
\end{aligned} \tag{4.2}$$

where $\frac{d\sigma_{q\bar{q}}}{d^2\mathbf{b}} = 2[1-\text{Re}\ S(x,r,b)]$ is the dipole-proton differential scattering cross

section, with $\mathbf{b}$ being the impact parameter. The first-kind Bessel function is denoted by J_0. Here $\sigma_{q\bar{q}}$ is the dipole-proton scattering cross section, which can be related to the forward scattering amplitude $N(x, r, b)$ for the dipole-proton system. The scattering amplitude will come from the solution of the dipole evolution equation, in our case, the BK equation.

The differental cross section for the production of final state vector mesons, given by

$$\frac{d\sigma_{T,L}^{\gamma^* p\to Vp}}{dt} = \frac{R_g^2}{16\pi}\left|\mathcal{A}_{T,L}^{\gamma^* p\to Vp}\right|^2\left(1+\beta^2\right), \tag{4.3}$$

where β is the ratio of real to imaginary parts of the scattering amplitude used to determine the real part of the scattering amplitude and is given by

$$\beta = \tan(\pi\lambda/2), \quad \lambda = \frac{\partial \ln\left(\mathcal{A}_{T,L}^{\gamma^* p\to Vp}\right)}{\partial \ln(1/x)}. \tag{4.4}$$

The skewed effect is reflected by R_g^2, given by [46]

$$R_g = \frac{2^{2\lambda+3}}{\sqrt{\pi}}\frac{\Gamma(\lambda+5/2)}{\Gamma(\lambda+4)}. \tag{4.5}$$

For the exponential dependence of t on the scattering amplitude $\mathcal{A}_{T,L}^{\gamma^* p\to Vp}$ [47], one can rewrite Eq. (4.3) as follows:

$$\frac{d\sigma_{T,L}^{\gamma^* p\to Vp}}{dt}(x, Q^2, t) = \frac{R_g^2}{16\pi}\left|\mathcal{A}_{T,L}^{\gamma^* p\to Vp}\right|^2_{t=0}\left(1+\beta^2\right)e^{-B_D|t|}, \tag{4.6}$$

where B_D denotes the area size of the interaction region, which can be obtained with a fit to the t-ditributions of the form $d\sigma/dt \propto \exp(-B_D|t|)$. The total scattering cross section is then obtained as

$$\sigma_{tot}^{\gamma^* p\to Vp}(x, Q^2) = \sigma_T^{\gamma^* p\to Vp}(x, Q^2) + \sigma_L^{\gamma^* p\to Vp}(x, Q^2), \tag{4.7}$$

with

$$\sigma_{T,L}^{\gamma^* p \to Vp}(x, Q^2) = \frac{R_g^2}{16\pi B_D} \Big| \mathcal{A}_{T,L}^{\gamma^* p \to Vp} \Big|_{t=0}^2 \Big(1 + \beta^2\Big). \tag{4.8}$$

For the ρ^0 vector meson, B_D is given by [47]

$$B_D = N\Big(14.0\Big(\frac{1GeV^2}{Q^2 + M_V^2}\Big)^{0.2} + 1\Big), \tag{4.9}$$

with $N = 0.55\, GeV^{-2}$ and $M_V = 0.776\, GeV$ for the ρ^0 meson. For the J/Ψ vector meson, B_D is given by [48]

$$B_D = \begin{cases} 4.15 + 4 \times 0.116 \ln\left(\frac{W}{W_0}\right), & Q^2 \leq 1\, GeV^2 \\ 4.72 + 4 \times 0.07 \ln\left(\frac{W}{W_0}\right), & Q^2 > 1\, GeV^2 \end{cases}, \tag{4.10}$$

where $W_0 = 90\, GeV$ and W is center of mass energy for $\gamma^* p$ system, related to x and Q^2 by

$$x = x_{Bj}\Big(1 + \frac{M_V^2}{Q^2}\Big) = \frac{Q^2 + M_V^2}{W^2 + Q^2}, \tag{4.11}$$

where x_{Bj} is the Bjorken scale and $M_V = 3.097\, GeV$ for J/Ψ vector meson.

4.2.2 Vector Meson Wavefunctions

One of the key ingredients to measuring the production of exclusive vector mesons is the overlap wave function $(\Psi_V^* \Psi)_{T,L}$, which is a function of the longitudinal momentum fraction z carried by the quark, the dipole size r, and the virtuality of the photon Q^2. In the literature, there are many different prescriptions for the overlap wavefunction between the photon and the vector meson, such as the DGKP (Dosch-Gousset-Kulzinger-Pirner) model [49], the Gaus-Light Cone (GLC) [30], and the boosted Gaussian (BG) model [50], first proposed by Nemchik et. al [51, 52]. The overlap function between the photon and the vector meson wave functions can

be written as

$$(\Psi_V^*\Psi)_T = \hat{e}_f e \frac{N_c}{\pi z(1-z)} \{m_f^2 K_0(\epsilon r)\phi_T(r,z) - [z^2+(1-z)^2]\epsilon K_1(\epsilon r)\partial_r \phi_T(r,z)\}, \tag{4.12}$$

$$(\Psi_V^*\Psi)_L = \hat{e}_f e \frac{N_c}{\pi} 2Qz(1-z)K_0(\epsilon r)\Big[M_V\phi_L(r,z) + \delta \frac{m_f^2 - \Delta_r^2}{M_V z(1-z)}\phi_L(r,z)\Big], \tag{4.13}$$

where $\hat{e}_f$ is the effective charge ($\hat{e}_f = 2/3, 1/\sqrt{2}$ for J/Ψ and ρ mesons, respectively.), $e = \sqrt{4\pi\alpha_{em}}$, N_c $(= 3)$ is the number of colors, $\Delta_r^2 = (1/r)\partial_r + \partial_r^2$, $\epsilon = \sqrt{z(1-z)Q^2 + m_f^2}$ (m_f is the quark mass), and K_0 and K_1 are the second kind Bessel function. ϕ_T and ϕ_L are the scalar parts of the overlap wave functions.

The vector meson wave functions are constrained by model-independent features. Firstly, it should satisfy the following normalization condition:

$$\sum_{h,\bar{h}} \int d^2\mathbf{r} \int_0^1 \frac{dz}{4\pi} \Big|\Psi_{h,\bar{h}}^V(z,\mathbf{r})\Big|^2 = 1 \tag{4.14}$$

Here, $\Psi_{h,\bar{h}}^V(z,\mathbf{r})$ represents the light-cone wave function of the vector meson with quark and antiquark helicities labeled by h and $\bar{h}$, respectively. The above normalization condition neglected the possible contributions of gluon or sea-quark states to the vector meson wave function, assuming that the quantum numbers of the meson are saturated by the quark-antiquark pair. For the scalar parts of the vector meson wave functions, the normalization conditions are [51, 52]

$$\frac{N_c}{2\pi}\int_0^1 \frac{dz}{z^2(1-z)^2}\int d^2\mathbf{r}\ \{m_f^2\phi_T^2 + [z^2+(1-z)^2]\ (\partial_r\phi_T)^2\} = 1, \tag{4.15}$$

$$\frac{N_c}{2\pi}\int_0^1 dz \int d^2\mathbf{r}\ \Big[M_V\phi_L + \delta\frac{m_f^2-\Delta_r^2}{M_V z(1-z)}\phi_L\Big]^2 = 1. \tag{4.16}$$

In addition to that, another important constraint comes from the leptonic decay width

$\Gamma(V \to e^+e^-)$, given by

$$f_{V,T} = \hat{e}_f \frac{N_c}{2\pi M_V} \int_0^1 \frac{dz}{z^2(1-z)^2} \ \{m_f^2 - [z^2 + (1-z)^2]\Delta_r^2\} \ \phi_T(r,z)\Big|_{r=0} \ , \quad (4.17)$$

$$f_{V,L} = \hat{e}_f \frac{N_c}{\pi} \int_0^1 dz \ \left[M_V + \delta \frac{m_f^2 - \Delta_r^2}{M_V z(1-z)}\right] \ \phi_L(r,z)\Big|_{r=0} \ , \quad (4.18)$$

where f_V is the coupling of the meson to the electromagnetic current obtained from the measured electronic decay width by

$$\Gamma_{V\to e^+e^-} = \frac{4\pi\alpha_{em}^2 f_V^2}{3M_V}. \quad (4.19)$$

For the completeness of the vector meson wave functions, Eqs. (4.12) and (4.13), the scalar parts ($\phi_{T,L}$) should be mentioned. In this work, we employ the BG and GLC models for the scalar part wave functions as they provide a better description of existing experimental data using the constraints given in Eqs. (4.15), (4.16), (4.17), and (4.18). We set $\delta = 0$ in the GLC model and $\delta = 1$ in the BG model, following the work done by Kowalski et. al. [31].

The scalar-part wave functions in the GLC model are given by

$$\begin{aligned} \phi_T(r,z) &= N_T[z(1-z)]^2 \exp(-r^2/2R_T^2), \\ \phi_L(r,z) &= N_L z(1-z) \exp(-r^2/2R_L^2). \end{aligned} \quad (4.20)$$

The parameters of the GLC model are given in Table 4.1.

Meson	M_V/GeV	f_V	m_f/GeV	N_T	R_T^2/GeV^{-2}	N_L	R_L^2/GeV^{-2}
J/Ψ	3.097	0.274	1.4	1.23	6.5	0.83	3.0
ρ^0	0.776	0.156	0.14	4.47	21.9	1.79	10.4

Table 4.1: Parameters of the GLC model for J/Ψ and ρ^0 vector mesons [44].

The scalar-part wave functions in the BG model are given by

$$\begin{aligned}\phi_T(r,z) &= \mathcal{N}_{\mathcal{T}} z(1-z)\exp\Big(-\frac{m_f^2\mathcal{R}^2}{8z(1-z)}-\frac{2z(1-z)r^2}{\mathcal{R}^2}+\frac{m_f^2\mathcal{R}_T^2}{2}\Big),\\ \phi_L(r,z) &= \mathcal{N}_{\mathcal{L}} z(1-z)\exp\Big(-\frac{m_f^2\mathcal{R}^2}{8z(1-z)}-\frac{2z(1-z)r^2}{\mathcal{R}^2}+\frac{m_f^2\mathcal{R}_L^2}{2}\Big).\end{aligned} \tag{4.21}$$

The parameters of the BG model are given in Table 4.2. We include these two

Meson	M_V/GeV	f_V	m_f/GeV	$\mathcal{N}_{\mathcal{T}}$	$\mathcal{N}_{\mathcal{L}}$	${\mathcal{R}_{\mathcal{T}}}^2/GeV^{-2}$	${\mathcal{R}_{\mathcal{L}}}^2/GeV^{-2}$
J/Ψ	3.097	0.274	1.4	0.578	0.575	2.3	2.3
ρ^0	0.776	0.156	0.14	0.911	0.853	12.9	12.9

Table 4.2: Parameters of the BG model for J/Ψ and ρ^0 vector mesons [44].

models into our calculations for vector meson production, which exhibit minimal sensitivity to the specified vector meson wave functions, and analyze the impact of both models on the outcomes. To facilitate visualization, we illustrate the transverse and longitudinal overlaps between the vector meson and photon wave functions as a function of the dipole size r at $z = 1/2$ $(0 < z < 1)$ in Figure 4.2.

4.3 Results and Discussion

This section presents the numerical results for the cross sections for the production of J/Ψ and ρ^0 vector mesons as a function of various scales involved in the process $\gamma^* p \to Vp$. We have provided the theoretical calculations of the differential and total cross sections for the electro-production of J/Ψ and ρ^0 vector mesons. Furthermore, we have shown the ratios of the longitudinal to transverse cross sections that are responsive to the vector meson wavefunctions. In the computation of cross sections, Eqs. (4.6), (4.7), (4.8), we primarily require two pieces of information: the dipole-proton scattering amplitude and the overlap wave functions for the vector mesons. We utilized the solution of the BK equation from the second chapter for the dipole-

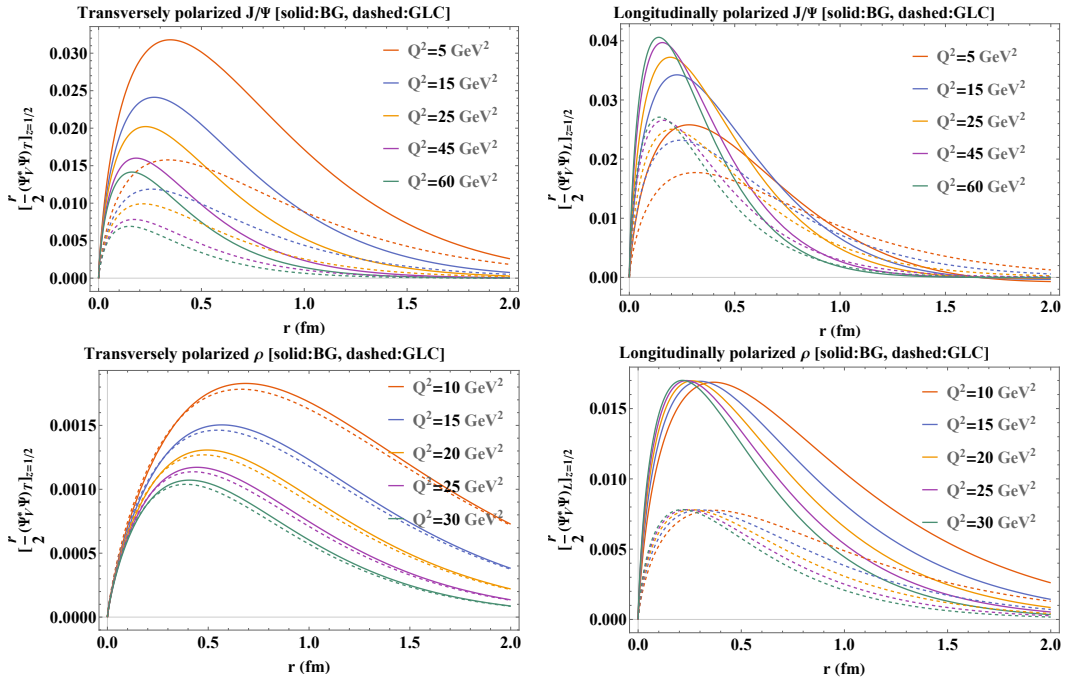

Figure 4.2: Overlap function between the photon and the vector meson wave functions [Eqs. (4.12) and (4.13)], as a function of dipole size r at $z = 1/2$ for various Q^2 values.

proton scattering amplitude. We utilized two renowned models, the Gaus-LC and the BG models, for the overlap wave functions. This document illustrates the impact of these two models on the estimates of cross-sections for the electro-production of specific vector mesons. We compared our theoretical predictions with the available experimental data to validate our approach.

The initial analysis presents the differential cross section results for the production of J/Ψ and ρ^0 vector mesons as a function of the squared momentum transfer t across various Q^2 values of experimental data. The results, together the comparison with the experimental data, are presented in Figures 4.3 and 4.4. The relationship between the total cross sections of J/Ψ and ρ^0 vector meson production and the center-of-mass energy of the $\gamma^* p$ system W for different Q^2 values is illustrated in Figures 4.5 and 4.6, respectively. Figure 4.5 illustrates the total cross-section for the production of the exclusive J/Ψ vector meson as a function of W at the highest accessible energy. The computed exclusive vector meson production aligns

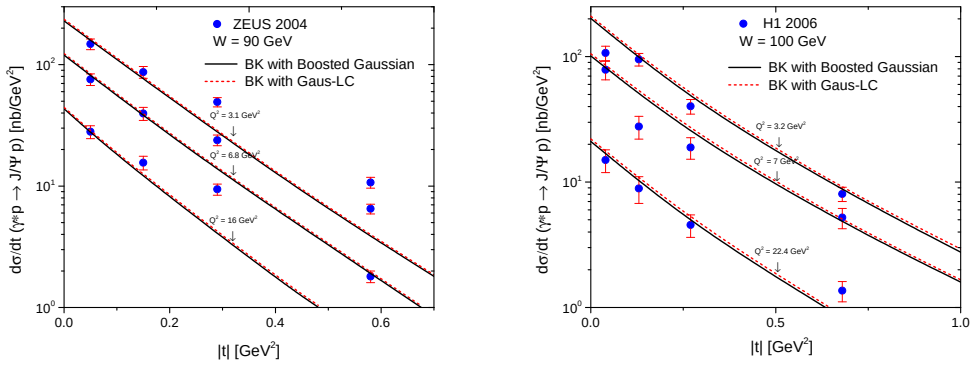

Figure 4.3: Differential cross section $d\sigma/dt(\gamma^* p \to J/\Psi\ p)$ vs. $|t|$ calculated using the solution of the BK equation with two different vector meson wave functions compared with the experimental data from ZEUS 2004 [20] at $W = 90$ GeV (left) and H1 2006 [22] at $W = 100$ GeV (right).

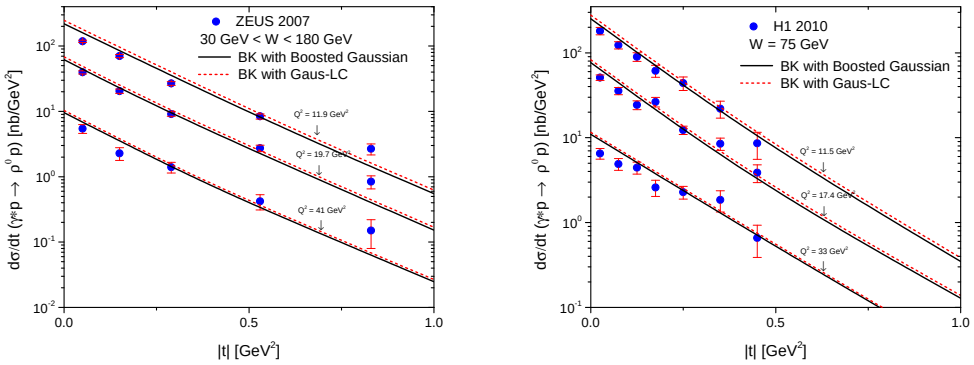

Figure 4.4: Differential cross section $d\sigma/dt\ (\gamma^* p \to \rho^0 p)$ vs. $|t|$ calculated using the solution of the BK equation with two different vector meson wave functions compared with the experimental data from ZEUS 2007 [23] for 30 GeV $< W <$ 180 GeV(left) and H1 2010 [24] at $W = 75$ GeV (right).

well with the existing experimental evidence. The results presented are somewhat contingent upon the two vector meson wave function models, namely the Gaus-LC and BG models. Figure 4.2 illustrates the discrepancies between these two models that influence the calculations of vector meson production. For the transversely polarized ρ^0, the Gaus-LC and BG models are identical, in contrast to other vector meson components. Nonetheless, they yield analogous predictions for vector meson generation using our solution the BK equation.

In the second analysis, we measured the total cross section, σ, for the production

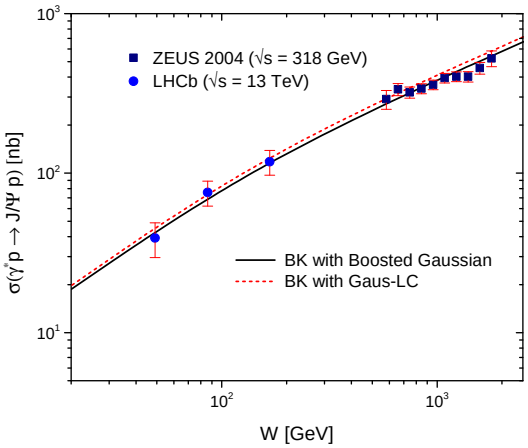

Figure 4.5: Total cross section $\sigma(\gamma^* p \to J/\Psi\ p)$ vs. W calculated using the solution of the BK equation with two different vector meson wave functions compared with experimental data from ZEUS 2004 [20] and LHCb [26].

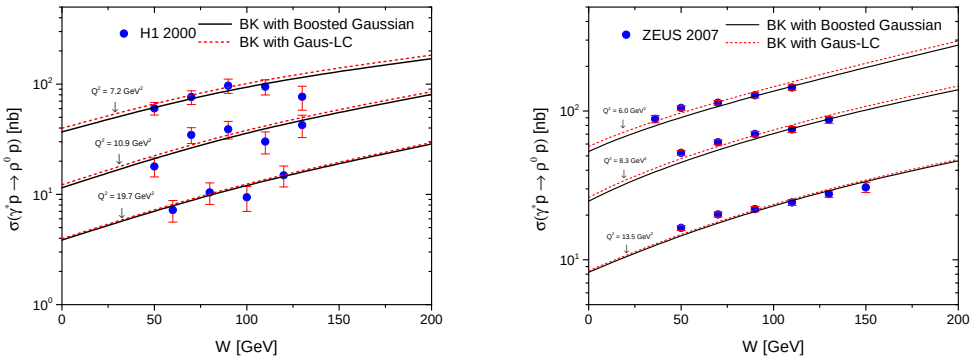

Figure 4.6: Total cross section $\sigma(\gamma^* p \to \rho^0 p)$ vs. W calculated using the solution of the BK equation with two different vector meson wave functions compared with experimental data at various Q^2 values from H1 2000 [19] (left) and ZEUS 2007 [23] (right).

of J/Ψ and ρ^0 vector mesons as a function of Q^2. The left plot of Figure 4.7 illustrates the total cross section for J/Ψ production at $W = 90$ GeV, whereas the right plot depicts the total cross section for ρ^0 production at $W = 75$ GeV. The theoretical predictions align closely with the current experimental results.

We have ultimately shown the ratio of longitudinal to transverse cross sections, $R = \sigma_L/\sigma_T$, as a function of Q^2 at a constant W. Figure 4.8 illustrates that the production ratio for the J/Ψ vector meson is directly proportional to Q^2, whereas

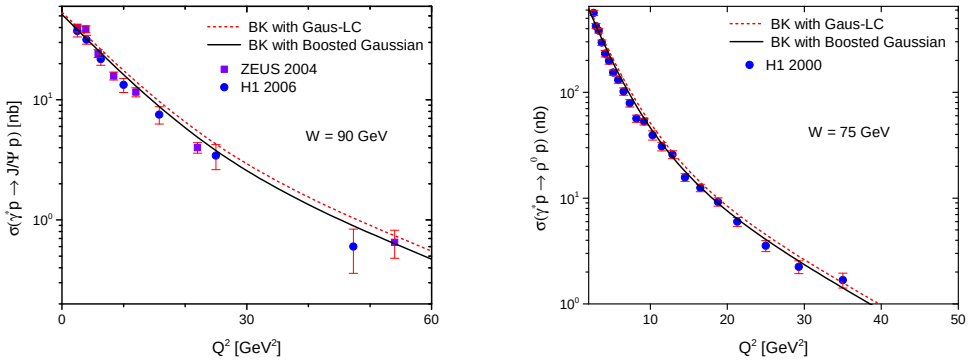

Figure 4.7: Total cross section σ vs. Q^2 calculated using the solution of the BK equation with two different vector meson wave functions. (left) For J/Ψ meson at $W = 90$ GeV compared with experimental data from ZEUS 2004 [20] and H1 2006 [22]. (right) For ρ^0 meson at $W = 75$ GeV compared with the data from H1 2000 [19] and ZEUS 2007 [23].

the production ratio for the ρ^0 vector meson increases significantly with rising Q^2. As Q^2 grows for both vector mesons, significant disparities emerge between the two vector meson wave function models. Consequently, the ratio exhibits significant sensitivity to the specified vector meson wave function models at elevated Q^2.

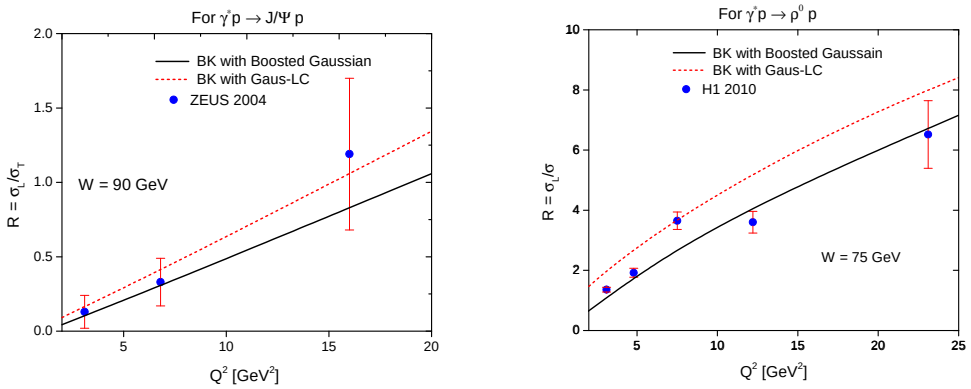

Figure 4.8: The ratio R vs. Q^2 calculated using the solution of the BK equation with two different vector meson wave functions: (left) R for J/Ψ meson at $W = 90$ GeV compared with the data from ZEUS 2004 [20] and (right) R for ρ^0 meson at $W = 75$ GeV compared with the data from H1 2010 [24].

4.4 Summary

This chapter examines exclusive vector meson production using the color dipole framework of DIS. We computed the cross-sections for the production of J/Ψ and ρ^0 vector mesons as functions of t, W, and Q^2 utilizing an analytical solution of the BK equation or the BK evolution theory. To corroborate our study, we compared the theoretical predictions for the cross-sections of J/Ψ and ρ^0 vector meson production with extant actual data, observing a satisfactory concordance between them. Our inquiry commenced with a succinct examination of the color dipole framework of DIS for vector meson production. In this context, we presented the scattering amplitude for vector meson production. This amplitude necessitated two fundamental components for vector meson production: the vector meson wavefunctions and the dipole-proton scattering amplitude. Utilizing two established models, the Gaus-LC and the BG, for the vector meson wave functions and deriving the dipole-proton scattering amplitude from the solution of the BK equation, we calculated the cross-sections for the production of J/Ψ and ρ^0 vector mesons, as well as the ratios of longitudinal to transverse cross-sections.

The findings indicate that our analytical solution to the BK equation accurately calculates vector meson production in a modest Q^2 range. The BK equation exhibits strong performance in low Q^2 and small-x regions. Nonetheless, with elevated Q^2, it is essential to include corrections from the DGLAP evolution equation in the calculations. Nevertheless, our analytical technique is applicable for quantifying vector meson cross-sections within the designated range. Furthermore, our findings underscore the susceptibility of results to the Gaus-LC and BG models. Although the disparities among these models become less apparent for the ρ^0 meson as Q^2 escalates, discrepancies are clearly observable for the J/Ψ meson, even at elevated Q^2 values. Furthermore, the ratios of longitudinal to transverse cross-sections for

the production of J/Ψ and ρ^0 vector mesons exhibit a notable dependence on the two wave function models as Q^2 escalates. Our investigations indicate that the answers derived from solving the BK equation using the BG model offer a superior representation of the data compared to those obtained from the Gaus-LC model.

The production of vector mesons is an effective approach to investigate the characteristics of nuclear materials. Our analytical solution to the BK equation can facilitate more phenomenological studies at both current and prospective experimental sites. We expect that diffractive processes, such as exclusive vector meson production at upcoming experimental facilities, will illuminate various facets of QCD.

Bibliography

[1] Jacob J Ethier and Emanuele R Nocera. Parton distributions in nucleons and nuclei. *Annual Review of Nuclear and Particle Science*, 70(1):43–76, 2020.

[2] Francise D Aaron, H Abramowicz, I Abt, L Adamczyk, M Adamus, Al-daya Martin, C Alexa, V Andreev, S Antonelli, P Antonioli, et al. Combined measurement and qcd analysis of the inclusive e±p scattering cross sections at hera. *Journal of High Energy Physics*, 2010(1):1–63, 2010.

[3] Halina Abramowicz, I Abt, L Adamczyk, M Adamus, V Andreev, S Antonelli, B Antunović, V Aushev, Y Aushev, A Baghdasaryan, et al. Combination of measurements of inclusive deep inelastic e^ ± p e±p scattering cross sections and qcd analysis of hera data: H1 and zeus collaborations. *The European Physical Journal C*, 75:1–98, 2015.

[4] Marcel Froissart. Asymptotic behavior and subtractions in the mandelstam representation. *Physical Review*, 123(3):1053, 1961.

[5] Edmond Iancu and Raju Venugopalan. The color glass condensate and high energy scattering in qcd. In *Quark–Gluon Plasma 3*, pages 249–363. World Scientific, 2004.

[6] Francois Gelis, Edmond Iancu, Jamal Jalilian-Marian, and Raju Venugopalan. The color glass condensate. *Annual Review of Nuclear and Particle Science*, 60(1):463–489, 2010.

[7] Jean-Paul Blaizot. High gluon densities in heavy ion collisions. *Reports on Progress in Physics*, 80(3):032301, 2017.

[8] A Accardi, JL Albacete, M Anselmino, N Armesto, EC Aschenauer, Alessandro Bacchetta, D Boer, WK Brooks, T Burton, N B Chang, et al. Electron-ion

collider: The next qcd frontier: Understanding the glue that binds us all. *The European Physical Journal A*, 52:1–100, 2016.

[9] JL Abelleira Fernandez, C Adolphsen, Ahmet Nuri Akay, H Aksakal, JL Albacete, S Alekhin, P Allport, V Andreev, RB Appleby, E Arikan, et al. A large hadron electron collider at cern report on the physics and design concepts for machine and detector. *Journal of Physics G: Nuclear and Particle Physics*, 39(7):075001, 2012.

[10] P Agostini, H Aksakal, S Alekhin, PP Allport, N Andari, KDJ Andre, D Angal-Kalinin, S Antusch, L Aperio Bella, L Apolinario, et al. The large hadron–electron collider at the hl-lhc. *Journal of Physics G: Nuclear and Particle Physics*, 48(11):110501, 2021.

[11] Daniele P Anderle, Valerio Bertone, Xu Cao, Lei Chang, Ningbo Chang, Gu Chen, Xurong Chen, Zhuojun Chen, Zhufang Cui, Lingyun Dai, et al. Electron-ion collider in china. *Frontiers of Physics*, 16:1–78, 2021.

[12] Leonid Vladimirovič Gribov, Eugene M Levin, and Michail G Ryskin. Semihard processes in qcd. *Physics Reports*, 100(1-2):1–150, 1983.

[13] Alfred H Mueller and Jianwei Qiu. Gluon recombination and shadowing at small values of x. *Nuclear Physics B*, 268(2):427–452, 1986.

[14] Alfred H Mueller. Parton saturation at small x and in large nuclei. *Nuclear Physics B*, 558(1-2):285–303, 1999.

[15] K Goeke, Maxim V Polyakov, and M Vanderhaeghen. Hard exclusive reactions and the structure of hadrons. *Progress in Particle and Nuclear Physics*, 47(2):401–515, 2001.

[16] Andrei V Belitsky and AV Radyushkin. Unraveling hadron structure with generalized parton distributions. *Physics reports*, 418(1-6):1–387, 2005.

[17] Heikki Mäntysaari. Review of proton and nuclear shape fluctuations at high energy. *Reports on Progress in Physics*, 83(8):082201, 2020.

[18] Spencer R Klein and Heikki Mäntysaari. Imaging the nucleus with high-energy photons. *Nature Reviews Physics*, 1(11):662–674, 2019.

[19] H1 Collaboration and C Adloff. Elastic electroproduction of mesons at hera. *The European Physical Journal C-Particles and Fields*, 13(3):371–396, 2000.

[20] S Chekanov, M Derrick, JH Loizides, S Magill, S Miglioranzi, B Musgrave, J Repond, R Yoshida, Margarita CK Mattingly, N Pavel, et al. Exclusive electroproduction of j/ψ mesons at hera. *Nuclear Physics B*, 695(1-2):3–37, 2004.

[21] Krzysztof Piotrzkowski, S Chekanov, and J de Favereau. Exclusive electroproduction of phi mesons at hera. *Nuclear Physics, Section B*, 718(1):3, 2005.

[22] Adil Aktas, Simon Baumgartner, Niklaus Berger, Marc A Del Degan, Wolfram Erdmann, Christoph Grab, Guillaume Leibenguth, Benno List, Salvatore Mangano, David Meer, et al. Elastic j/ψ production at hera. *The European Physical Journal C*, 46(3):585–603, 2006.

[23] ZEUS Collaboration gallo@ mail. desy. de. Exclusive ρ 0 production in deep inelastic scattering at hera. *PMC Physics A*, 1:1–47, 2007.

[24] Francise D Aaron, M Aldaya Martin, C Alexa, V Andreev, B Antunovic, A Asmone, S Backovic, A Baghdasaryan, E Barrelet, W Bartel, et al. Diffractive electroproduction of ρ and ϕ mesons at hera. *Journal of High Energy Physics*, 2010(5):1–111, 2010.

[25] Roel Aaij, C Abellan Beteta, A Adametz, B Adeva, M Adinolfi, C Adrover, A Affolder, Ziad Ajaltouni, J Albrecht, F Alessio, et al. Exclusive j/ψ and ψ (2s) production in pp collisions at tev. *Journal of Physics G: Nuclear and Particle Physics*, 40(4):045001, 2013.

[26] Roel Aaij, Bernardo Adeva, Marco Adinolfi, Christine Angela Aidala, Ziad Ajaltouni, Simon Akar, Pietro Albicocco, Johannes Albrecht, Federico Alessio, Michael Alexander, et al. Central exclusive production of j/ψ and ψ (2s) mesons in pp collisions at $\sqrt{s} = 13$ tev. *Journal of High Energy Physics*, 2018(10):1–27, 2018.

[27] K Golec-Biernat and M Wüsthoff. Saturation effects in deep inelastic scattering at low q 2 and its implications on diffraction. *Physical Review D*, 59(1):014017, 1998.

[28] Alfred H Mueller. Unitarity and the bfkl pomeron. *Nuclear Physics B*, 437(1):107–126, 1995.

[29] Edmond Iancu, K Itakura, and S Munier. Saturation and bfkl dynamics in the hera data at small-x. *Physics Letters B*, 590(3-4):199–208, 2004.

[30] Henri Kowalski and Derek Teaney. Impact parameter dipole saturation model. *Physical Review D*, 68(11):114005, 2003.

[31] G Watt and H Kowalski. Impact parameter dependent color glass condensate dipole model. *Physical Review D—Particles, Fields, Gravitation, and Cosmology*, 78(1):014016, 2008.

[32] VP Goncalves, Magno Valério Trindade Machado, and Anelise Ramires Meneses. Non-linear qcd dynamics and exclusive production in ep collisions. *The European Physical Journal C*, 68:133–139, 2010.

[33] Nikolai N Nikolaev and BG Zakharov. Colour transparency and scaling properties of nuclear shadowing in deep inelastic scattering. *Zeitschrift für Physik C Particles and Fields*, 49(4):607–618, 1991.

[34] Alfred H Mueller. Soft gluons in the infinite-momentum wave function and the bfkl pomeron. *Nuclear Physics B*, 415(2):373–385, 1994.

[35] Alfred H Mueller and Bimal Patel. Single and double bfkl pomeron exchange and a dipole picture of high energy hard processes. *Nuclear Physics B*, 425(3):471–488, 1994.

[36] Krzysztof Golec-Biernat and Anna M Staśto. On solutions of the balitsky–kovchegov equation with impact parameter. *Nuclear Physics B*, 668(1-2):345–363, 2003.

[37] D Bendova, J Cepila, JG Contreras, and M Matas. Solution to the balitsky-kovchegov equation with the collinearly improved kernel including impact-parameter dependence. *Physical Review D*, 100(5):054015, 2019.

[38] T Lappi and H Mäntysaari. Direct numerical solution of the coordinate space balitsky-kovchegov equation at next-to-leading order. *Physical Review D*, 91(7):074016, 2015.

[39] Marek Matas, Jan Cepila, and Jesus Guillermo Contreras Nuno. Numerical precision of the solution to the running-coupling balitsky-kovchegov equation. In *EPJ Web of Conferences*, volume 112, page 02008. EDP Sciences, 2016.

[40] J Cepila, JG Contreras, and M Matas. Collinearly improved kernel suppresses coulomb tails in the impact-parameter dependent balitsky-kovchegov evolution. *Physical Review D*, 99(5):051502, 2019.

[41] Ranjan Saikia, Pragyan Phukan, and Jayanta Kumar Sarma. An analytical solution of balitsky–kovchegov equation using homotopy perturbation method. *International Journal of Modern Physics A*, 37(31n32):2250190, 2022.

[42] Ranjan Saikia, Pragyan Phukan, and Jayanta Kumar Sarma. Investigation of proton structure function at hera in light of an analytical solution to the balitsky–kovchegov equation. *Communications in Theoretical Physics*, 76(3):035202, 2024.

[43] Jeffrey Berger and Anna M Stasto. Exclusive vector meson production and small-x evolution. *Journal of High Energy Physics*, 2013(1):1–26, 2013.

[44] H Kowalski, L Motyka, and G Watt. Exclusive diffractive processes at hera within the dipole picture. *Physical Review D—Particles, Fields, Gravitation, and Cosmology*, 74(7):074016, 2006.

[45] Jochen Bartels, K Golec-Biernat, and Krisztian Peters. On the dipole picture in the nonforward direction. *arXiv preprint hep-ph/0301192*, 2003.

[46] AG Shuvaev, Krzysztof J Golec-Biernat, Alan D Martin, and MG Ryskin. Off-diagonal distributions fixed by diagonal partons at small x and ξ. *Physical Review D*, 60(1):014015, 1999.

[47] Mohammad Ahmady, Ruben Sandapen, and Neetika Sharma. Diffractive ρ and ϕ production at hera using a holographic ads/qcd light-front meson wave function. *Physical Review D*, 94(7):074018, 2016.

[48] Jan Cepila, Jan Nemchik, Michal Krelina, and Roman Pasechnik. Theoretical uncertainties in exclusive electroproduction of s-wave heavy quarkonia. *The European Physical Journal C*, 79:1–29, 2019.

[49] Hans Gunter Dosch, T Gousset, G Kulzinger, and HJ Pirner. Vector meson leptoproduction and nonperturbative gluon fluctuations in qcd. *Physical Review D*, 55(5):2602, 1997.

[50] Jeffrey R Forshaw, R Sandapen, and Graham Shaw. Color dipoles and ρ, φ electroproduction. *Physical Review D*, 69(9):094013, 2004.

[51] J Nemchik, Nikolai N Nikolaev, and BG Zakharov. Scanning the bfkl pomeron in elastic production of vector mesons at hera. *Physics Letters B*, 341(2):228–237, 1994.

[52] J Nemchik, Nikolai N Nikolaev, E Predazzi, and BG Zakharov. Color dipole phenomenology of diffractive electroproduction of light vector mesons at hera. *Zeitschrift für Physik C Particles and Fields*, 75:71–87, 1997.